國立臺灣大學工學院機械工程學系

碩士論文

Department of Mechanical Engineering

College of Engineering

National Taiwan University

Master Thesis

簡諧震盪圓柱流場之閉迴路流體控制

Closed-loop Flow Control on Harmonic Oscillation of a Circular Cylinder

林靜得

Ching-Te Lin

指導教授: 蔡協澄 博士

Advisor: Hsieh-Chen Tsai, Ph.D.

中華民國 112 年 6 月

June, 2023

doi: 10.6342/NTU202301391

doi: 10.6342/NTU202301391

國立臺灣大學碩士學位論文
口試委員會審定書
MASTER'S THESIS ACCEPTANCE CERTIFICATE
NATIONAL TAIWAN UNIVERSITY

（論文中文題目）(Chinese title of Master's thesis)

簡諧震盪圓柱流場之閉迴路流體控制

（論文英文題目）(English title of Master's thesis)

Closed-loop Flow Control on Harmonic Oscillation of a Circular Cylinder

本論文係___林靜得_____(姓名)_R10522108__（學號）在國立臺灣大學機械工程學系研究所完成之碩士學位論文，於民國 112 年 06 月 30 日承下列考試委員審查通過及口試及格，特此證明。

The undersigned, appointed by the Department / Institute of Mechanical Engineering on 30 (date) June (month) 2023 (year) have examined a Master's thesis entitled above presented by Lin, Ching-Te (name)_R10522108_ (student ID) candidate and hereby certify that it is worthy of acceptance.

口試委員 Oral examination committee:

蔡明潤	周逸儒	張鈞棣
（指導教授 Advisor）		
李宇修		

系主任/所長 Director: 林沛群

Acknowledgements

能夠準時完成畢業論文是每個研究生的夢想，但在碩一結束跟老師提出這篇論文的初步想法時，我其實心中可以說是毫無把握，原因無他，想要在圓柱流場實現閉迴路控制是一個我從大四就想要實現的作法，但翻遍論文跟反覆檢視任何可能發生錯誤的地方後，我依然連最基本的 Vortex Shedding 都無法完全控制。因此有幸按照文章內的方法達成初步的結果，雖然結果仍然不近完美，依然有改進的空間，但能夠達成這個里程碑，肯定要感謝很多人。首先要感謝從大學專題就開始指導我的蔡協澄老師，也可以說是我踏入計算流體以及流體控制研究的啟蒙者，沒有老師每週 meeting 的鼓勵跟建議我應該沒有辦法完成這篇論文，更不用說在寫完這篇致謝文的一個月後去讀博了。

另外也要感謝這次論文口試的口委教授們，感謝周逸儒教授、張鈞棣教授以及李宇修教授願意在百忙之中撥空擔任我的口試委員，非常感謝教授們在學術上的建議，以及寫作上的改進方向，讓我有機會將這篇論文完整出版。感謝實驗室學長學弟妹們的協助，謝謝新雨學長帶我進入 CFD 的世界，謝謝丁豪學長跟我一起完成大四時的研究，以及昱銘學長在實驗室協助大大小小的事情。感謝旻霖學長一起完成了碩一的研究，也在申請的路上互相鼓勵，祝我們都可以順利完成博班學業。感謝昱豪，王昱，哲維，立瑄這兩年一起在實驗室討論研究，以及給我在教學上的建議。

感謝遠在員林的父母以及家人，沒有你們 24 年的支持這條路我不可能走得下去。

林靜得謹記

中華民國 112 年 7 月 15 日

doi: 10.6342/NTU202301391

doi: 10.6342/NTU202301391

摘要

本研究旨在應用閉迴路流場控制降低圓柱於均勻流場中進行簡諧震盪產生的升力波動。通過此不可壓縮流的數值模擬的時間平均基流，可將於圓柱附體座標系下的納維-斯托克斯方程式進行線性化。再利用預解分析推導出此流場的線性系統模型，藉此設計出兩個線性反饋控制方案。首先，採用迴路整型法 (loop-shaping method) 設計出可最大化穩定裕度及抵抗來自週期性邊界條件的干擾的強韌控制器。數值模擬結果顯示, 此控制方案可減少升力波動達 5.7%。再者，引入模型參考自適性控制 (model reference adaptive control) 以處理系統因加入控制器帶來的時變化。本研究採用直接型控制以直接更新時變的自適應控制增益。結果顯示，自適應控制成功降低了 30.9% 的升力波動。

關鍵字：流場控制、預解分析、強韌控制、自適性控制

doi: 10.6342/NTU202301391

doi: 10.6342/NTU202301391

Abstract

In this study, closed-loop flow control is implemented in order to attenuate the lift fluctuation of a circular cylinder oscillating harmonically in a uniform stream. Through the numerical simulation of the incompressible flow around the oscillating cylinder, a time-invariant base flow is obtained by averaging the flow over time to linearize the incompressible Navier-Stokes equations in the cylinder-fixed frame. A resolvent-analysis-based model derived from the linearized equations is used to design two linear feedback control schemes. First, the loop-shaping method is adopted to design a robust controller that maximizes the stability margin and rejects the disturbance imposed by the periodic boundary condition. The simulation shows this control scheme can reduce the lift fluctuation by 5.7%. Furthermore, the model reference adaptive control is introduced to deal with time-varying linear plant due to the addition of the controller. A direct approach of this control is adopted to directly update the time-varying adaptive control gains. The results show that the adaptive controller successfully reduce the lift fluctuation by 30.9%. ◦

Keywords: Flow control, Resolvent analysis, Robust control, Adaptive control

doi: 10.6342/NTU202301391

doi: 10.6342/NTU202301391

Contents

doi: 10.6342/NTU202301391

doi: 10.6342/NTU202301391

List of Figures

doi: 10.6342/NTU202301391

doi: 10.6342/NTU202301391

Denotation

Γ	The first learning rate for the adaptive gains
γ	The second learning rate for the adaptive gains
θ	Angle from stagnation point to actuator position
θ_c	Adaptive control time-varying parameters, $\theta_c = [c_0, \theta_1^T, \theta_2^T, \theta_3]^T$
ν	Kinematic viscosity
σ	Singular values of Resolvent operator
σ_g	The Width of 2D gaussian function g
σ_p	Plunging amplitude
ϕ	Right singular vector of Resolvent operator
ψ	Left singular vector of Resolvent operator
ω_n'	Perturbed vorticity in the non-inertia frame
ω_n	Vorticity in the non-inertia frame

doi: 10.6342/NTU202301391

A	linear time-invariant matrix of the dynamic system formed by linearized Navier-Stokes equation
a	The peak frequency of the second-order weighting function for the loop-shaping method
$B(x, y)$	forcing matrix of the dynamic system
$\mathcal{C}$	CFL number $C = \frac{u_{\max}\Delta t}{\Delta x}$
C	Sensing matrix in a SISO system
D	Diameter of the cylinder
f_a	Control amplitude generated by the feedback controller
f_u	nonlinear forcing
f_p	Plunging frequency
$g(\sigma_g, r, \theta_c)$	2D Gaussian function
k	The gain of the weighting function for the loop-shaping method
$P(s)$	The SISO transfer function between the control input to the sensing velocity
$R(\omega)$	Resolvent operator, $(-i\omega - A)^{-1}$
$\mathcal{R}_x$	The relative fluctuation reduction quantity for the time-series data x
St^*	Strouhal number of peak frequencies in the Resolvent analysis
St_p	Strouhal number of plunging frequencies, $St_p = f_p D/U_\infty$

doi: 10.6342/NTU202301391

St_{vs}	Strouhal number of natural shedding frequencies
u_n	Velocity in the non-inertia frame
u'_n	Perturbed velocity in the non-inertia frame
u_p	The control input of the model reference adaptive control
U_p	The plunging velocity of the cylinder
U_∞	Free stream velocity

doi: 10.6342/NTU202301391

doi: 10.6342/NTU202301391

Chapter 1 Introduction

Flow control is a new-rising research topic due to its applications in a wide range of engineering systems (such as drag reduction of the bluff body and channel flow, lift enhancement of aircraft design, and laminar-turbulent transition). Particularly, feedback flow control has the potential to achieve the goals of robustness and adaptiveness in practical application. To accomplish the performance requirement, feedback flow control utilizes multidisciplinary knowledge, including dynamic systems, control theory, and fluid mechanics. To my best knowledge, this field's research effort mainly focuses on flow fields with stationary boundaries. However, most engineering systems are regarding moving boundaries, such as a rotating wind turbine. Hence, there is an urge to explore possible flow control methods for such cases. Considering the complexity of free-moving rigid body boundaries and the computational cost of the required fluid-structure-interaction (FSI) simulation, a periodic moving boundary is chosen to study in this thesis.

1.1 Flow Control Methods

Flow control can be, in general, divided into two categories: passive and active control. Passive flow control utilizes the modification of surfaces to achieve control require-

doi: 10.6342/NTU202301391

ments. Several researchers utilized passive methods for the drag reduction of the channel flow. Endrikat *et al.*[6] showed the optimal shape of riblets to achieve drag reduction with the Kelvin-Helmholtz instability. In addition, Gómez-de-Segura & García-Mayoral. [11] showed that permeable substrates are a possible solution to reduce turbulent drag.

On the other hand, active flow control methods alter the flow field by employing actuators normally placed on the boundaries. Open-loop controls, which apply harmonic forcing via direct body forces or thermal actuators, have shown profound success in drag reduction. Gatti & Quadrio[9] investigated the influence of increasing Reynolds number on the skin-friction drag reduction via a spanwise-harmonic forcing on the walls of a channel flow. Moreover, Quadrio *et al.* [23] reported that only a proper speed of forward-traveling wave of the wall oscillation affects drag reduction. Conversely, the backward-traveling wave has the reducing-drag effect at any speed. Besides the application of the internal flow, previous studies also showed the potential of the external flow. Sipp [25] indicated that the high-frequency harmonic forcing on the laminar cavity flow is capable of stabilizing the global mode, which behavior is described by the Stuart–Landau equation.

Moreover, the actuator output could also be determined by the feedback laws about a chosen measurement, such as the transverse velocity in the cylinder wake. These feedback flow control methods could be designed based either on model-free approaches or an identified plant, which captures the major dynamics of the fluid flows. First of all, the model-free approaches are widely used in either the internal flow or the external flow. In internal flow, the most well-known feedback flow control was the opposition control, which sets up a blow/suction wall boundary condition to oppose the wall-normal velocity at a certain distance from the wall [2][13]. The methodology creates a ”virtual” wall in the

doi: 10.6342/NTU202301391

near-wall region to lift the near-wall cycle and successfully reduce drag. As for the external flow, Son and Choi [27] performed the iterative tuning on the proportional-integral-differential (PID) controller to suppress the vortex shedding behind the circular cylinder under the Reynolds number of 60 and 100. With the optimization process, they ended with successful results in attenuating lift fluctuation and reducing mean drag. Recently, neural-network-based methods are gaining more attention due to the rising of computational power in the past decade. Rabault *et al.*[24] proposed a deep reinforcement learning scheme to discover the control strategies capable of stabilizing the Kármán vortex with the Reynolds number of 100. They achieved the desired outcome of stabilization of vortex shedding and the drag reduction of 8% with limited input mass flow rates of the actuators on the circular cylinder.

Secondly, the model-based controller synthesis relies on the identification of the plant to characterize the input-output relation of a given flow field. Typically, a linear model is preferred due to the commensurate control theories compared to the nonlinear control. In this thesis, the Resolvent operator, widely adopted in the community of flow control groups, is utilized to quantify the linear model in the wake flow. Hence, in the next section, Resolvent analysis will be introduced along with the reviews of previous research works done by this method.

1.2 Resolvent Analysis in Fluid Dynamics

Resolvent analysis has been proven as a powerful tool for identifying the amplification mechanism in the fluid system. McKeon and Sharma [20] first treated the nonlinear convective term in the linearized Navier-Stokes equation as nonlinear forcing to formulate the Resolvent analysis of a turbulent pipe flow. In this way, Resolvent analysis can be

doi: 10.6342/NTU202301391

represented as an input-output relation between nonlinear forcing and flow response. By examining the pseudo spectrum of Resolvent operator, they revealed the most amplified mode of wall-bound turbulence. This concept was also used in the study of opposition control to interpret the control capacity based on the mode revealed by Resolvent analysis [19]. Yeh and Taira [28] further extended this method to separation flow over an airfoil. They presented an open-loop control methodology for a thermal actuator on the leading edge, which implements periodic excitation on the optimal frequency based on the Resolvent analysis of time-averaged flow. Similar methods [18] [22] were also performed in the cavity flow and turbulent jets. Padovan *et al.* [21] purposed harmonic Resolvent to tackle the issue of a time-periodic base flow. The paper indicated the cross-frequency structure with the harmonic Resolvent. Recently, Skene *et al.* [26] proposed the $\mathcal{L}_1$ norm-based optimization on figuring out the spatially sparse forcing mode, providing the choice of actuator locations.

According to the former studies, the Resolvent analysis can reveal the critical structure of the fluid system and indicate the optimal frequency and position to implement open-loop control. Furthermore, the method provides a critical linear plant for the feedback controller design in the next section.

1.3 Model-based Feedback Flow Control

Model-based feedback flow control is advantageous for stability analysis with the understanding of the system. Therefore, this study focuses on designing a feedback controller based on the linear model. However, the intrinsic characteristics of fluid dynamics consist of high dimensions and nonlinearity. For an actual system, these properties result

doi: 10.6342/NTU202301391

in unmodeled dynamics and disturbance. Consequently, robust control and adaptive control are often utilized to adjust the controller to react with the real fluid system. First, robust control is favored in the flow control community for being able to reject disturbance from either the unmodeled nonlinearity in the predetermined linear plant or the measurement noise in the experimental studies. In recent decades, researchers leveraged this theory to develop a robust flow controller in various fluid flows. Flinois and Morgans (2016)[8] obtained the linear reduced-order model by the Eigensystem Realization Algorithm to design the controller for the unsteady flow of a bluff body. With the linear model, the controller was then devised via the $\mathcal{H}_\infty$ loop-shaping method. Jin *et al.*[15] showed that the Resolvent-based model was also available for the controller synthesis. They presented a loop-shaping approach to the vortex shedding suppression's controller design problem. Leclercq *et al.* (2019)[16] developed an iterative algorithm by updating the mean flow required for the Resolvent-based linear model. They successfully suppressed the intrinsic oscillation in the open cavity flow within five stages. The idea of updating the linear model to adjust to the unknown plant is similar to the adaptive control concept. Hence, several previous studies of adaptive flow control have been conducted to investigate the capacity of adaptive control when interacting with fluid dynamics. Fabianne *et al.* [7] obtained an adaptive controller via the adaptive filtered-X least-mean-squares (FXLMS) algorithm to adapt to various Reynolds numbers to diminish the two-dimensional TS wave growth. Hu and Morgans[12] presented an alternative adaptive algorithm, the LMS algorithm, for attenuating the unsteady loading of high-rising buildings immersed in the atmospheric boundary layer. Furthermore, online-estimating models were explored to enhance the adaptivity of the controller. Deem *et al.* [5] applied the online Dynamic Mode Decomposition (DMD) to adjust the estimated model for the boundary layer separation control. To

doi: 10.6342/NTU202301391

summarize, these successes in applying advanced control theory motivate us to explore effective control approaches by extending the well-studied cases of stationary boundaries to the periodic-oscillating boundaries .

This paper will focus on designing a feedback flow controller on a plunging cylinder under the Reynolds number of 100. This research aims to attenuate the additional lift fluctuation caused by the plunging motion. In chapter 2, the complete analysis of the flow response of a plunging cylinder will be presented, including the mean and fluctuation of the force coefficients. In chapter 3, the estimated model and corresponding control methods will be introduced. The modal analysis of the given flow field is first analyzed by the Resolvent analysis. The instability will be investigated through the analysis to provide modeling information for control designing problems in the next stage. Moreover, two control theories have been applied to fulfill the objective: robust and adaptive control. In chapter 4, the comprehensive comparative study between the two control approaches and the uncontrolled flow will be examined thoroughly. Lastly, chapter 5 concludes this thesis and proposes future works.

doi: 10.6342/NTU202301391

Chapter 2 Plunging Oscillation of a Circular Cylinder at a Low Reynolds Number

In this thesis, a transversely oscillating circular cylinder is chosen as an example of periodic-moving boundaries. The harmonic motions of the boundaries introduce additional fluctuation to the flow field, which is originally unsteady due to the vortex shedding. Overall, the proposed control schemes in the following chapter aim to alleviate the fluctuation. Before designing the suitable controller, the flow physics behind a plunging cylinder should be examined to determine the proper setting for the numerical experiment.

In this chapter, the parametric study regarding the plunging cylinder is discussed in order to determine suitable examples to implement feedback actuators on the cylinder. Harmonic oscillations of bluff bodies have been widely investigated to understand their unsteady response in various industrial applications. Choi *et al.*[3] demonstrated the surging and plunging oscillations of an airfoil at a Reynolds number of 300. They showed the lock-in phenomenon in two types of harmonic motions, as well as its effect on the force coefficient. Bao *et al.*[1] further examined the effect of a transversely oscillating cylinder and of two tandem cylinders. However, the data in the paper about a single oscillating cylinder is inadequate in the search for ideal parameters of plunging motions to implement

doi: 10.6342/NTU202301391

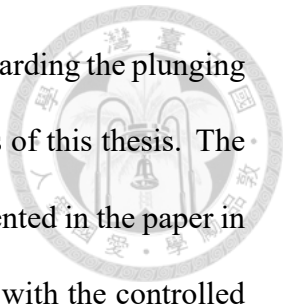

control on it. Therefore, it is inevitable that a detailed investigation regarding the plunging amplitudes and frequencies has to be performed for the completeness of this thesis. The force and unsteady flow structure under harmonic oscillation are presented in the paper in order to quantify the uncontrolled flow. The result is then compared with the controlled flow in the following two chapters. In section 2.1, the problem setup is discussed, and the applied numerical method is also presented. In section 2.2, the mean forces and the fluctuation are shown, which are significantly altered by the unsteady motion of the rigid-body boundary. Lastly, in section 2.3, the lock-in phenomenon is discussed. Within the lock-in region, the flow response of the circular cylinder synchronizes with the unsteady motion under a specific setting.

2.1 Problem Setup and Numerical Method

A circular cylinder plunging in an unbounded free stream serves as an example of periodic motion in this paper. Numerical simulation is utilized to obtain the flow field at a low Reynolds number $Re = U_\infty D/\nu = 100$, where U_∞ is the incoming flow velocity, D is the diameter of the cylinder, and ν is the kinematic viscosity. Among a plethora of industry-oriented cases of periodic-moving boundaries, the case of plunging cylinder is a simple but general case to study as it possesses several features of an unsteady flow, including separation, vortex shedding, and shear layer. Therefore, one could expect that the result of this paper can be applied to various other flow fields at low Reynolds numbers. Due to the low Reynolds number, the flow around the cylinder was quasi-two-dimensional. Hence, the simulation could be conducted in two dimensions, which is set to be the cross-section of the cylinder. For the numerical method, the immersed boundary projection method (IBPM) developed by Colonius and Taira[4] is adopted, which utilizes a null space

doi: 10.6342/NTU202301391

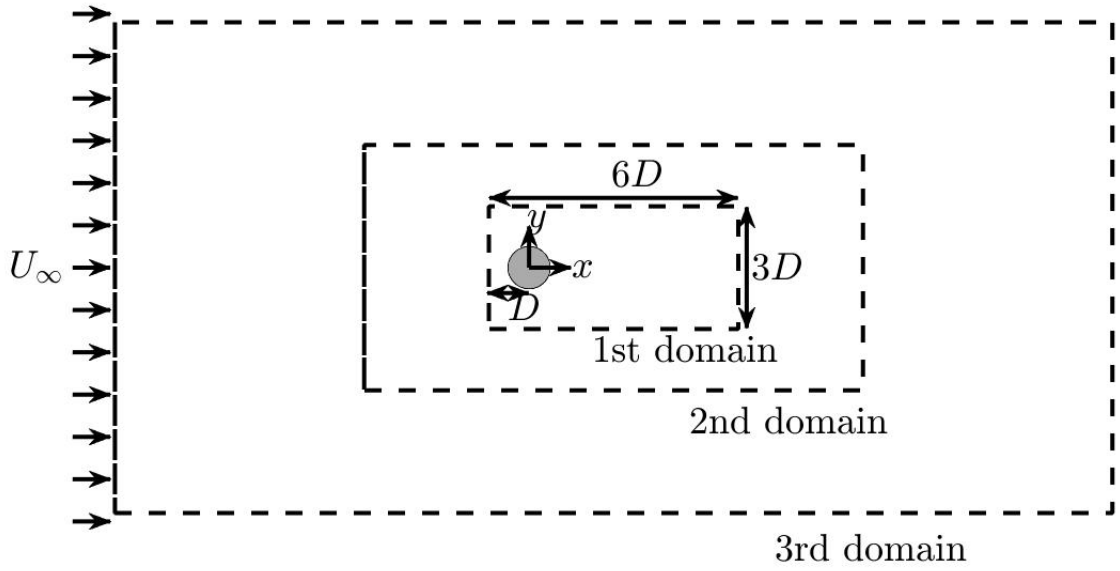

Figure 2.1: Schematic figure of 3-level multi-domain method

approach and multi-domain far-field boundary condition. IBPM is implemented to solve the two-dimensional incompressible Navier-Stokes in the non-inertial frame of the cylinder derived by Lin *et al.*[17]. Vorticity is chosen as the primary variable to solve, and the no-slip boundary condition was satisfied by exerting body forces on the boundary points. The far-field boundary condition is by setting the vorticity as zero.

$$\begin{aligned} &\frac{\partial \omega_n}{\partial t} = \nabla \times \left[(u_n - U_p) \times \omega_n\right] - \frac{1}{Re}\nabla \times (\nabla \times \omega_n) \\ &\begin{cases} u_n = U_p \text{ on the cylinder} \\ u_n \to \hat{x},\ \omega_n \to 0 \text{ at infinity} \end{cases}, \end{aligned} \tag{2.1}$$

where U_p is the plunging velocity to be described below, and $\hat{x}$ is the unit vector. The simulation is performed in six levels of the computation domain, with the grid-coarsifying factor of 2 at each level. Figure 2.1 shows the schematic graph of the multi-domain. The periodically plunging cylinder with diameter D in uniform incoming flow U_∞ is placed

doi: 10.6342/NTU202301391

in the first (finest) domain with a length of $6D$ in the streamwise direction and a width of $3D$ in the transverse direction. The center of the cylinder is placed at $1D$ from the left boundary and $1.5D$ from the bottom boundary. The numerical scheme is discretized with an equal grid spacing $\Delta x = \Delta y = 0.05D$. The time-marching step Δt is set to keep the CFL number, $\mathcal{C} = \frac{u_{\max}\Delta t}{\Delta x}$, less than 0.4.

The periodic motion of the cylinder is defined by the plunging amplitude σ_p and frequency f_p. The Strouhal number for plunging is defined as $St_p = f_p D/U_\infty$. Hence, the kinematic equation of the cylinder is $U_p = \sigma_p \omega_p \cos(\omega_p t)\hat{y}$, where $\omega_p = 2\pi St_p$ was the dimensionless angular velocity, and $\hat{y}$ was the transverse unit vector. In sections 2.2 and 2.3, the effect of different settings of σ_p and f_p on the force coefficient and the lock-in phenomenon, will be discussed.

2.2 Lift and Drag Coefficient

In this section, the induced force exerted on the cylinder due to the plunging motion is investigated. In general, the force response is greatly influenced by the lock-in phenomenon from the perspective of lift or drag coefficient. The lift C_L and drag coefficient C_D are defined as

$$C_L = \frac{F_y}{\frac{1}{2}\rho U_\infty^2},\ C_D = \frac{F_x}{\frac{1}{2}\rho U_\infty^2}, \tag{2.2}$$

where F_x, F_y are the total forces exerted on the cylinder in the x and y directions, respectively, and ρ stands for the density. To eliminate the transient response in computation, the data is collected for 50 periods of plunging oscillation after the first 10 periods.

Discussion of the time-series data would focus mainly on the time average and its standard deviations. The two statistics figures represent the total forces and the fluctuation

doi: 10.6342/NTU202301391

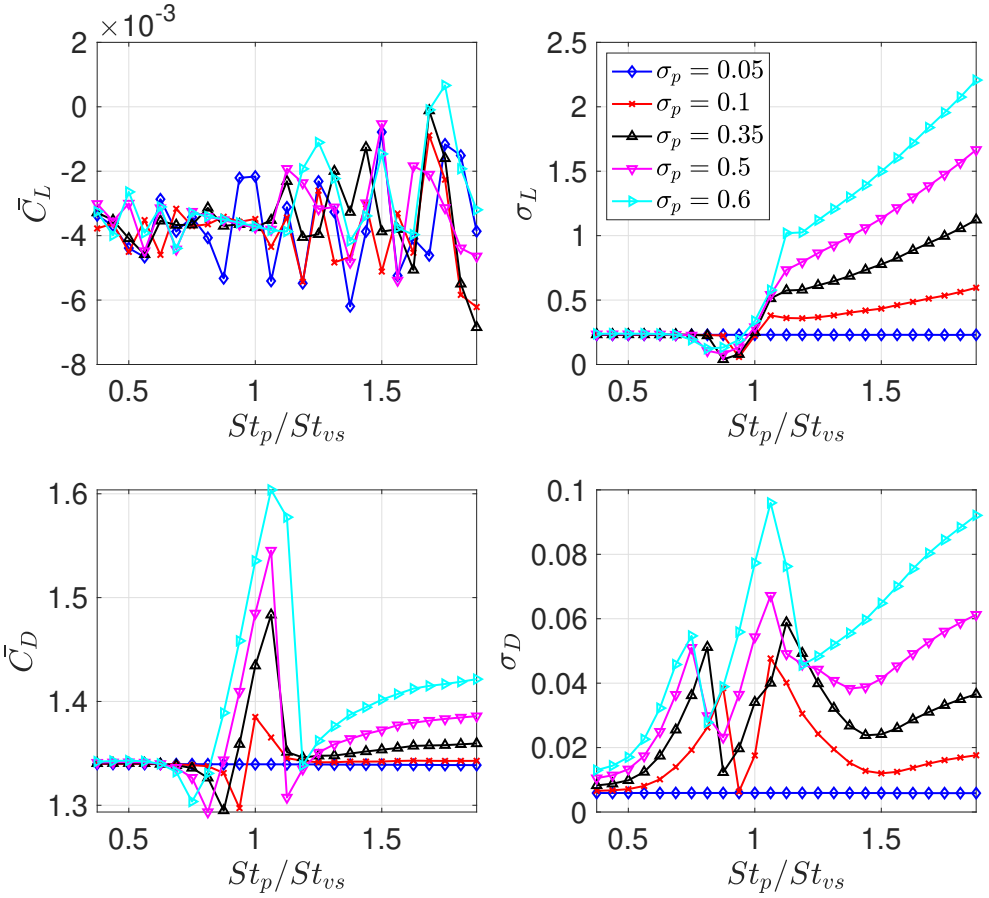

Figure 2.2: Time-average $\bar{C_L}$ $\bar{C_D}$ and standard deviation $\sigma_L, \sigma_D$of lift and drag coefficient

doi: 10.6342/NTU202301391

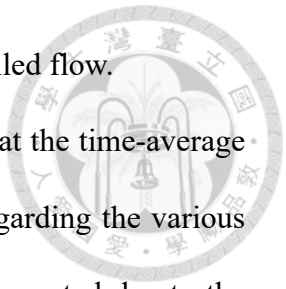

respectively, which could later be indicated as the objective of controlled flow.

First, considering the time-average force coefficient, it is apparent that the time-average lift coefficient $\bar{C_L}$ in figure 2.2 does not show a significant trend regarding the various sets of plunging amplitudes and frequencies. This result could be expected due to the symmetry oscillating motion in the transverse direction. Therefore, the long-term mean of the lift force is expected to approach zero regardless of plunging amplitudes and frequencies. However, the drag force shows a disparate outcome. Mean drag force reaches its maximum around the shedding frequencies St_{vs} at various amplitudes. Then, a gradual increment can be seen when the plunging frequency St_p is larger than the shedding frequency, especially in the plunging amplitude σ_p of 0.6.

Second, the standard deviation in figure 2.2 also shows different stories on lift and drag coefficients. The standard deviation of lift force, denoted as σ_L, amplifies greatly while the plunging frequency is larger than the natural shedding frequency. Moreover, the amplification mechanism strengthens with respect to the increase in the plunging amplitudes. The deviation of drag force has an overall increase across different frequencies. Although two peaks are observed near natural shedding frequency St_{vs} and the 0.7 of St_{vs}, the absolute value is far smaller than the deviation of the lift coefficient. The result shows that the major fluctuation induced by the oscillating motion strengthens the lift coefficient fluctuation. To conclude, the fact provides a solid reason to set the control objective as attenuating lift coefficient fluctuation over the control horizon.

2.3 Lock-in Phenomenon

In the previous section, I have shown that both force coefficients strongly correlate with the natural shedding frequency. This effect is known as the lock-in phenomenon.

doi: 10.6342/NTU202301391

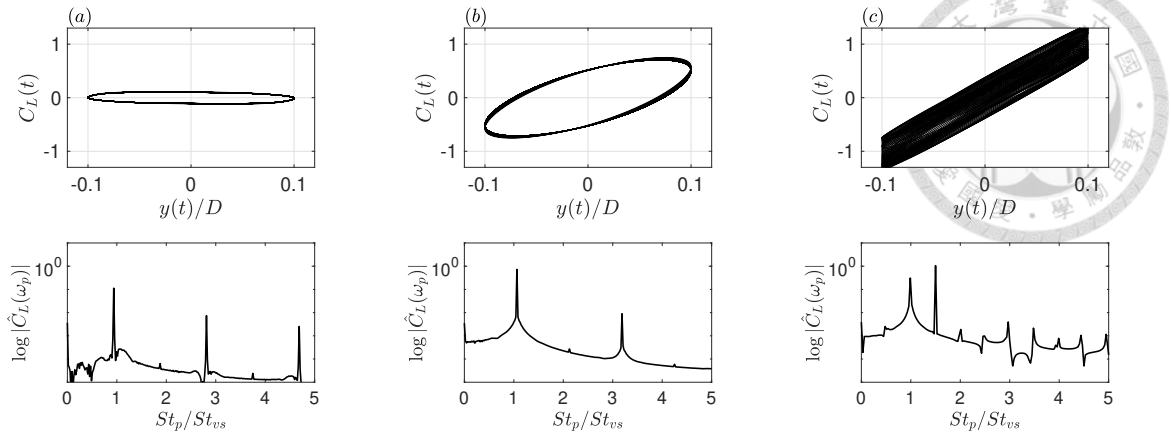

Figure 2.3: Plunging cases with lock-in (a,b) and without lock-in(c). Plunging amplitude σ_p is fixed to 0.1, and the phase portrait and the spectrum of lift coefficient are shown with respect to various plunging frequencies, where $(a)\ St_p/St_{vs} = 0.9375$,$(b)\ St_p/St_{vs} = 1.0625$,$(c)\ St_p/St_{vs} = 1.5$. $St_{vs} = 0.16$

In general, the lock-in phenomenon is defined as the dominant frequencies of the flow response are only the harmonics of the oscillating frequency. In figure 2.3, three representative cases are displayed. The cases of normalized plunging frequency $St_p/St_{vs} = 0.9375$ and 1.0625 are examples of limit-cycle-type trajectories in the phase portrait of the lift coefficient versus the normalized displacement $y(t)/D$. The two cases are categorized as the lock-in phenomenon. Conversely, the cases of $St_p/St_{vs} = 1.5$ showed a quasi-periodic-type trajectory in the phase portrait. Apparently, the flow response consists of more than a single harmonic frequency. It is also revealed in the spectrum of the lift coefficient. In the lock-in case, the dominant frequencies are only located in the harmonics of the plunging frequencies, while the non-lock-in case shows multiple dominant frequencies along the whole spectrum.

For further discussion on the lock-in phenomenon, a criterion based on the dominant frequencies as follows is adopted. The dominant frequencies are chosen based on the magnitude of the lift spectrum, which is larger than 0.001. If the differences between the dominant frequencies and the harmonics of the plunging frequencies are less than 0.001, the case is defined as the lock-in phenomenon. Figure 2.4 shows the region of the lock-in

doi: 10.6342/NTU202301391

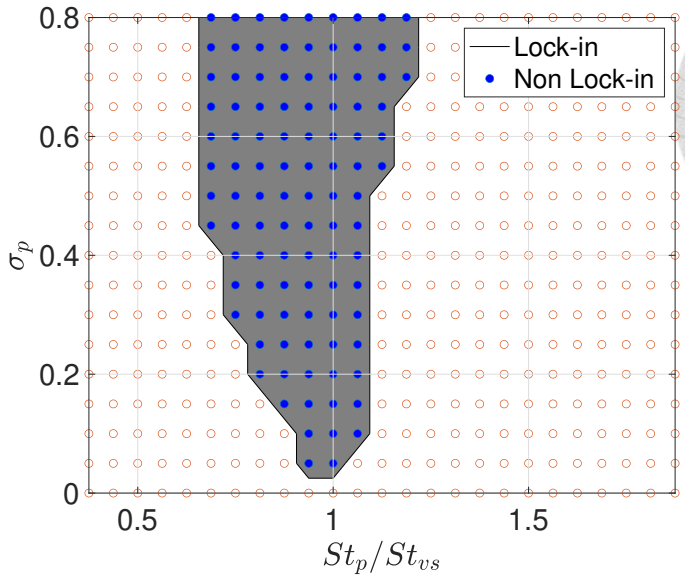

Figure 2.4: Lock-in area with respect to amplitudes σ_p and normalized frequencies St_p/St_{vs}

cases with respect to the plunging amplitudes and frequencies. The lock-in region concentrated at the natural shedding frequency St_{vs}. The area widens with the increase of the plunging amplitude σ_p. In general, the oscillation of the circular cylinder only induces a lock-in phenomenon near the shedding frequency.

To conclude, since the aim of this thesis is to show the capability of feedback control to stabilize the unsteady flow, a non-lock-in case is preferred with its intrinsic complexity and generality compared to the lock-in cases. Hence, the case of $\sigma_p = 0.1$ and $St_p/St_{vs} = 1.5$ is chosen to demonstrate the effect of the control laws proposed in the following chapters.

doi: 10.6342/NTU202301391

Chapter 3 Modal Analysis and Control Methods

In this chapter, the linear model analysis and control methods for the plunging cylinder are elucidated in detail. First, the modal analysis of the plunging cylinder wake flow is demonstrated and displayed in section 3.1. Specifically, for modal analysis, the Resolvent analysis is conducted to study the linear amplification mechanism of the flow field. Psuedospectrum and corresponding modes are shown in the section. After formulating the Resolvent operator, the dynamic model based on the operator can thus be constructed and forms a single-input-single-output system in section 3.2 for the following discussion. Furthermore, the control methods utilized in this thesis are elucidated in section 3.3 and 3.4. In section 3.3, the closed-loop characteristics are first shown with the critical transfer functions from the disturbance input to the system output. The result can thus be applied in the robust controller design via the loop shaping method. Lastly, the model reference adaptive control is introduced in section 3.4 to achieve the adaptive control for the oscillating flow field.

doi: 10.6342/NTU202301391

3.1 Resolvent Analysis

Resolvent analysis is utilized to establish the input-output relation of a linear system. Resolvent analysis is able to reveal the amplifying mechanism of the system under different frequencies of external forcing. In this paper, the linear system is constructed based on the linearization of non-inertial vorticity equation. In a non-inertial frame, the vorticity equation (2.1) was shown in the previous chapter. With averaged flow $\overline{u}_n(x), \overline{\omega}_n(x)$ and given velocities of boundaries $U_p(t)$, we can decompose the nonlinear PDE in equation(2.1)to linear periodic part and nonlinear part as equation(3.1).

$$\frac{\partial \omega_n'}{\partial t} = L(\overline{u}_n, \overline{\omega}_n)\omega_n' + N(\overline{u}_n, \overline{\omega}_n, \omega_n', U_p), \tag{3.1}$$

where $L(\overline{u}_n, \overline{\omega}_n)\omega_n' = \nabla \times \left[\overline{u_n} \times \omega' + u_n' \times \overline{\omega}_n - \frac{1}{Re}\nabla \times \omega_n'\right]$ and $N(\overline{u}_n, \overline{\omega}_n, \omega_n', U_p) = \nabla \times \left[(\overline{u}_n - U_p) \times \overline{\omega} + (u_n' - U_p) \times \omega_n' - \frac{1}{Re}\nabla \times \overline{\omega}_n\right]$. If we further regard the nonlinear term $N(\overline{u_n}, \overline{\omega_n}, \omega_n')$ in equation(3.1) as a forcing term in the linear system, the nonlinear system can be modeled as a linear system coupled with a nonlinear forcing f_u shown in equation (3.2).

$$\begin{aligned} &\frac{\partial \omega_n'}{\partial t} = L(\overline{u}_n, \overline{\omega}_n)\omega_n' + f_u \\ &u_n'(x_b) = U_p, \omega_n', u_n' \to 0, |x_r| \to \infty, \end{aligned} \tag{3.2}$$

where x_b is the solid boundary. Therefore, by spatially discretizing the vorticity field, the system can be denoted as the standard state-space form of the dynamic system.

$$\begin{aligned} &\frac{dx}{dt} = Ax + f \\ &\text{where } x = \omega_i, \end{aligned} \tag{3.3}$$

doi: 10.6342/NTU202301391

Since the linear system matrix A is time-invariant, the frequency response can be established by taking the Fourier transform of the linear system. Hence, the input-output relation between flow response and forcing at the given frequency could be constructed.

$$\begin{aligned} \hat{x}(\omega) &= (-i\omega - A)^{-1}\hat{f}(\omega) \\ x(t) &= \int_{-\infty}^{\infty} \hat{x}(\omega)e^{-i\omega t}d\omega \\ f(t) &= \int_{-\infty}^{\infty} \hat{f}(\omega)e^{-i\omega t}d\omega \end{aligned} \tag{3.4}$$

By evaluating the Resolvent matrix $R(\omega) = (i\omega - A)^{-1}$ in equation (3.4), the maximal amplification mechanism can be revealed via singular value decomposition (SVD) of the Resolvent matrix. Through SVD, the low-rank structure of the Resolvent matrix can be further built to shed light on the dominant amplifying modes and frequencies in the given flow field. Thus, the Resolvent can be approximated as the following equation.

$$R(\omega) = (-i\omega - A)^{-1} \approx \phi_{m\times k}\sigma(\omega)_{k\times k}\psi^*_{k\times m} \tag{3.5}$$

ϕ : first k columns of right singular vector , acting as response mode

$\sigma(\omega)$: first k terms of singular value , acting as gain of transfer function

ψ^* : first k columns of left singular vector , acting as forcing mode

In general, the linear operator A, which is linearized based on the Navier-Stokes equation, is non-normal. The non-normality causes the shift of the gain of the pseudospectrum from the eigenspectrum. This outcome leads to different amplifying frequencies compared with the most unstable eigenvalue of the linear operator A. Therefore, Resolvent analysis is essential to discover the response perturbed by the forcing, instead of simply computing the eigenspectrum and its mode. However, due to the low-Reynolds number constraint in

doi: 10.6342/NTU202301391

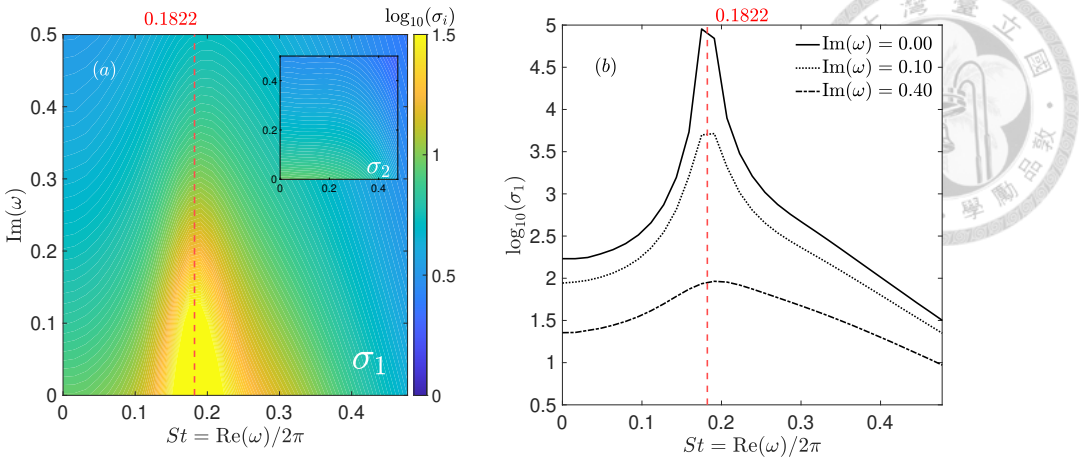

Figure 3.1: Contour plot of σ in different $\omega = \omega_r + i\omega_i$. The red dash line denotes the peak frequency St^* in Resolvent gain

.

this thesis, the pseudospectrum of the Resolvent operator presented in figure 3.1 does not possess a strong non-normal property. For the cases with a high-Reynolds number, the non-normal effect will be expected to be revealed with a similar analyzing procedure.

By examining the pseudospectrum and the modes, several characteristics of the flow field are revealed , which are keys to the control design in the following section. First, the first singular value σ_1 on the complex plane is compared with the second singular value σ_2. Apparently, the magnitude of σ_1 is an order larger than σ_2. It shows that the input-output relation could be approximated as the product of the first response and forcing mode times the gain $\sigma_1\phi_1\psi_1^*$. Second, the distribution of σ_1 shows a local maximum near the most unstable eigenvalue of linear operator A and stretches along the ω_i axis with a gradual descent. On the other hand, the magnitude of σ_1 decays fast along the ω_r axis. Lastly, one thing should be clarified. Since the system is still stable, there is no need to perform the finite-time approach, which is adopted in the study of the Resolvent analysis on a separated flow by Yeh and Taira (2019) [28].

The response modes and forcing modes are shown in figure 3.2. From the forcing mode of $St/St^* = 1$ at which the input force amplifies the most, the peak in the contour plot is

doi: 10.6342/NTU202301391

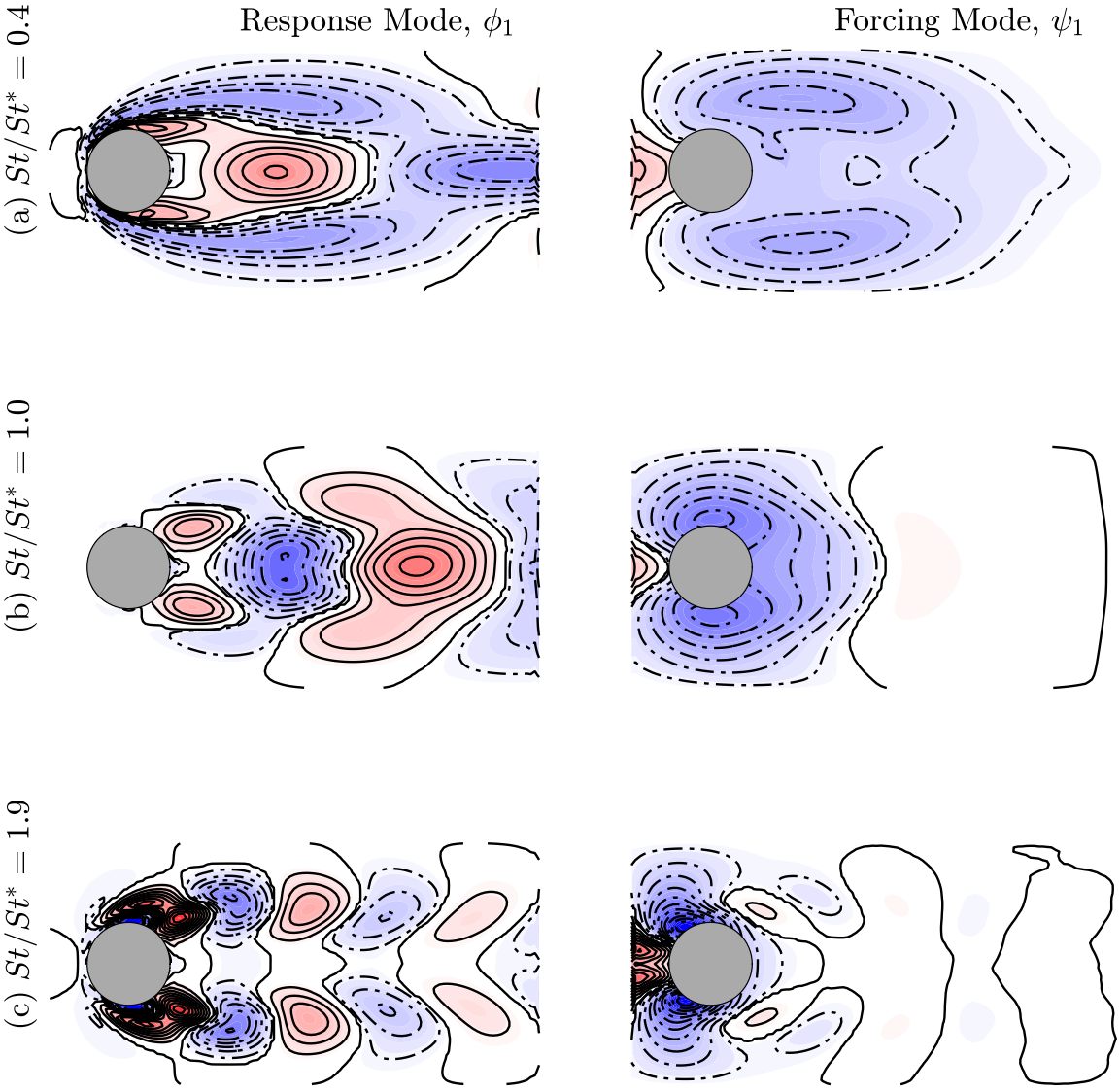

Figure 3.2: The leading response and forcing modes' real part at various perturbed frequencies St for $\mathrm{Im}(\omega) = 0$, $St/St^* = (a)0.4, (b)1.0, ;$ and $(c)1.9$ with $St^* = 0.1822$. Positive and negative vorticity contour levels are plotted respectively in solid and dash-dotted curves.

doi: 10.6342/NTU202301391

close to the trailing separation point. This fact supports the choice of actuation position on the separation point, $\theta = 110^\circ$, from the stagnation point to the actuating position. Moreover, the response mode on the peak frequency indicates a wake-type structure of the perturbed system. The structure implies the von-Karman wake behind the plunging cylinder.

To conclude, the linearized model sheds light on the critical amplification mechanism in the flow system to excite the instability phenomenon. However, due to its intrinsic characteristic of spatially discretized schemes, the system is high-dimensional, which is hard to apply in the control synthesis. Therefore, A reduced-order model is required to approximate the response of the high-dimensional system. The method will be presented in the section 3.2.

3.2 Dynamic Model of SISO system

In this section, the single-input-single-output (SISO) system is established to synthesize a controller to reject the disturbance introduced by the periodic motion of the rigid bodies. Forcing input in the given system will be modeled as body forces exerted on the fluid grids via a Gaussian function. In the control setup, the fluid system is forced by a pair of antisymmetric forces on the top and bottom sides of the cylinder, which mimics the effect of zero-net-mass actuators. The two body forces of blow/suction actuators are written in the following form.

$$
\begin{aligned}
f &= B(x,y) f_a, \\
B(x,y) &= \begin{pmatrix} \cos\theta_c (g(\sigma_g, r, \theta_c) - g(\sigma_g, r, -\theta_c)) \\ \sin\theta_c (g(\sigma_g, r, \theta_c) + g(\sigma_g, r, -\theta_c)), \end{pmatrix}
\end{aligned} \tag{3.6}
$$

doi: 10.6342/NTU202301391

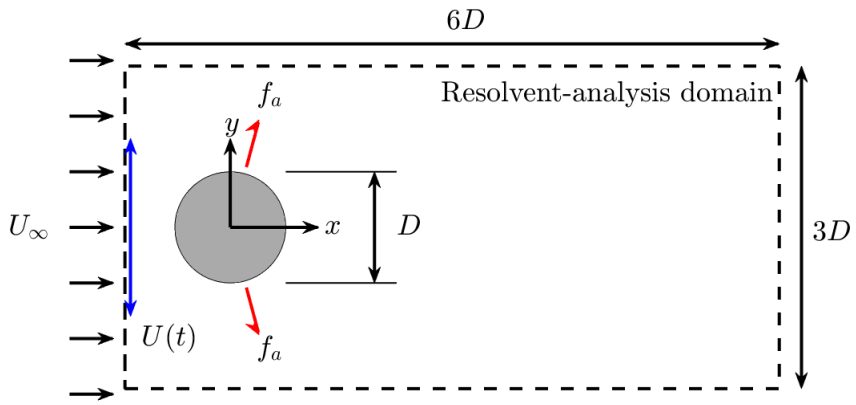

Figure 3.3: Schematic graph and computational domain with plunging cylinder

where f_a is the control amplitude generated by the feedback controller. θ_c is the angle between the actuators and the leading edge. $g(\sigma, r, \theta_c)$ is the unit 2D Gaussian function with width σ_g and centered at (r, θ_c).

$$g(\sigma_g, r, \theta_c) = \frac{1}{2\pi\sigma^2} \exp\Big(- \frac{(x - r\cos\theta_c)^2 + (y - r\sin\theta_c)^2}{2\sigma_g^2} \Big) \tag{3.7}$$

In this thesis, the actuator is located near the separation point of $(r, \theta_c) = (0.6, 110°)$, while the sensor is placed at $x = 1.0D$. The sensor is a velocity sensor to feedback the transverse velocity v to the designed controller. To simplify the discussion regarding various control methods, the sensor location is fixed at location $1D$ behind the cylinder. Since the state-space model is derived in the form of vorticity, output matrices C should be constructed by solving the Poisson equation. Lastly, the SISO system can be denoted as the following form.

$$\begin{aligned} \frac{dx}{dt} &= Ax + Bf_a \\ y &= Cx \\ \hat{y}(s) &= P(s)\hat{f}_a(s) \end{aligned} \tag{3.8}$$

doi: 10.6342/NTU202301391

In general, the transfer function $P(s)$ is high-dimensional due to the spatial discretization. However, it causes potential difficulties when computing control designing problems. Consequently, the reduced-order model (ROM) can be derived from the frequency response data obtained by the Resolvent analysis. MATLAB toolbox *fidfrd* is applied to identify the ROM $\tilde{P}(s)$ with the dimension of N, which is limited to the order of 10. With the ROM $\tilde{P}(s)$, robust control theory can then be introduced to design the feedback controller in the next section 3.3.

3.3 Characteristics of Closed-Loop Transfer Functions and Loop-shaping Method

The core concept of robust control is to design an optimal linear controller which is able to reject the disturbance caused by the uncertainty of the model. The method is especially widely used in the area of flow control because of the intrinsic nonlinear property of fluid dynamics. Our model is built based on the linearization of a nonlinear governing equation while treating the nonlinear part as an internal forcing. Therefore, the model is born to interact with the uncertainty of nonlinearity. By decomposing the forcing f into the external and internal forcing, f_a and f_u, the nonlinear system can be represented by a linear system coupled with uncertainty.

$$\begin{aligned} \frac{dx}{dt} &= Ax + Bf_a + f_u \\ y &= Cx \\ Y(s) &= C(i\omega - A)^{-1}\Big(Bf_a(s) + N_\Delta(x)\Big) \end{aligned} \tag{3.9}$$

The block diagram of the uncertain model is shown in figure 3.4. By connecting the con-

doi: 10.6342/NTU202301391

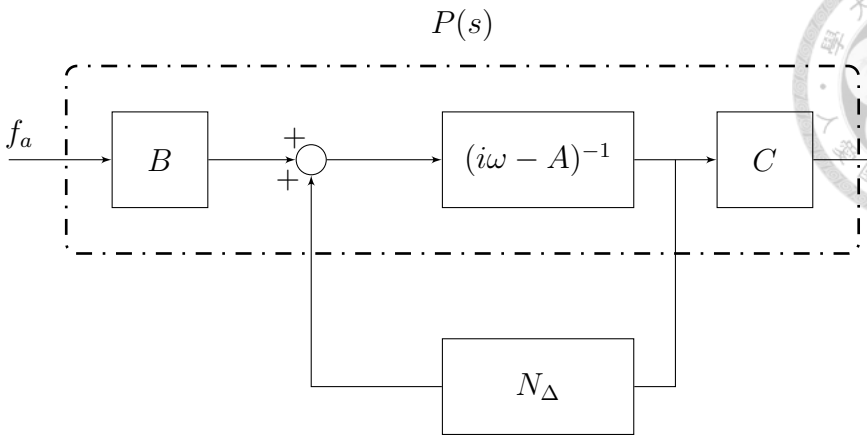

Figure 3.4: Block diagram of the model with uncertainty

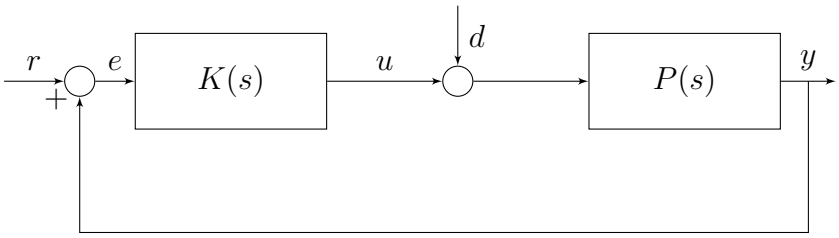

Figure 3.5: Block diagram of the closed-loop system

troller in the positive feedback loop, the uncertainty can be treated as the input disturbance d. The block diagram with the controller K is illustrated in figure 3.5, where

$$u = K(r - y). \tag{3.10}$$

With the positive feedback loop, the frequency response can be given by

$$Y = \frac{1}{1 - PK}(Kr + Pd) \tag{3.11}$$

In order to suppress the self-sustained oscillation due to the interaction between the Resolvent operator and the nonlinear forcing term, we have to first investigate the four key transfer functions to quantify the effect of the controller to reject disturbance in the framework of a positive closed-loop system. The closed loop is characterized by the four transfer

doi: 10.6342/NTU202301391

functions,

$$\begin{bmatrix} y \\ u \end{bmatrix} = \begin{bmatrix} T & PS \\ KS & T \end{bmatrix} \begin{bmatrix} r \\ d \end{bmatrix}, \tag{3.12}$$

which links the two inputs r, d, to two outputs y, u. The four transfer functions are not independent of each other. Instead, they are a combination of plant P and controller block K. To be more specific, two functions are introduced to compose the four transfer functions.

$$S = \frac{1}{1 - PK},\ T = \frac{PK}{1 - PK}, \tag{3.13}$$

where S is called the sensitivity function, and T is called the complementary sensitivity function. The two functions play important roles in quantifying the amplifying mechanism of the chosen system in response to various frequencies of disturbance. Therefore, by evaluating the frequency responses of the two functions, one could easily predict the effect of the linear controller, which will be constructed in the next section.

Specifically, in the paper, the controller's goal is to attenuate the fluctuation of the lift coefficient. In the formulation of the Resolvent operator, the nonlinear term along the periodic term caused by the periodic-oscillating motions is collected in the input disturbance d. The transfer function from d to y is

$$T_{d \to y} = PS \tag{3.14}$$

By investigating the spectrum of the nonlinear forcing $N_\Delta(x)$, the goal of attenuating fluctuation can be achieved by minimizing the gain of $T_{d \to y}$ in the identified frequencies, whereas the nonlinear forcing resulted in peaks in the spectrum of amplitude. The goal of gain-minimization can be accomplished through the method of loop shaping.

In the loop shaping method, the controller K is designed to achieve the specific character-

doi: 10.6342/NTU202301391

istics of the four closed-loop transfer functions in the equation (3.12). Before elucidating the method in the application, the $\mathcal{H}_\infty$-norm has to be first defined to continue the discussion. The $\mathcal{H}_\infty$-norm is defined as the maximum modulus of the frequency response. The infinity norm is established to quantify the robustness of the controlled system considering various disturbances.

$$||H||_\infty = \max_{\omega \in \mathbb{R}} |H(i\omega)| \tag{3.15}$$

In this thesis, I adopt the loop-shaping method of Glover & McFarlane (1989) [10] to design the controller by maximizing the coprime stability margin b.

$$b = || \begin{bmatrix} K \\ I \end{bmatrix} (I + PK)^{-1} \begin{bmatrix} P & I \end{bmatrix} ||_\infty^{-1} \tag{3.16}$$

In general, the margin b represents the robust characteristic of rejecting disturbance input to the controlled system. Hence, the larger the value is, the more robust the system is with the designed controller, which is expected to resist the disturbance introduced by the nonlinear forcing under the Resolvent formulation and, hence, attenuate the fluctuation sustained by the nonlinear forcing.

The optimization process is performed by the MATLAB toolbox *ncfsyn*. For the SISO plant, a compensator weight W should be determined prior to weight the plant with the control objective.

$$W(s) = k\frac{a^2}{(s+a)^2} \tag{3.17}$$

, where k is the gain of the weighting function, and a is the peak frequencies of the second-order filter. The parameters, k and a, are devised to achieve a sufficiently low gain of the closed-loop response on the dominant frequencies of the uncontrolled system, which are expected to be plunging frequency and its harmonics. The form of the compensator has

doi: 10.6342/NTU202301391

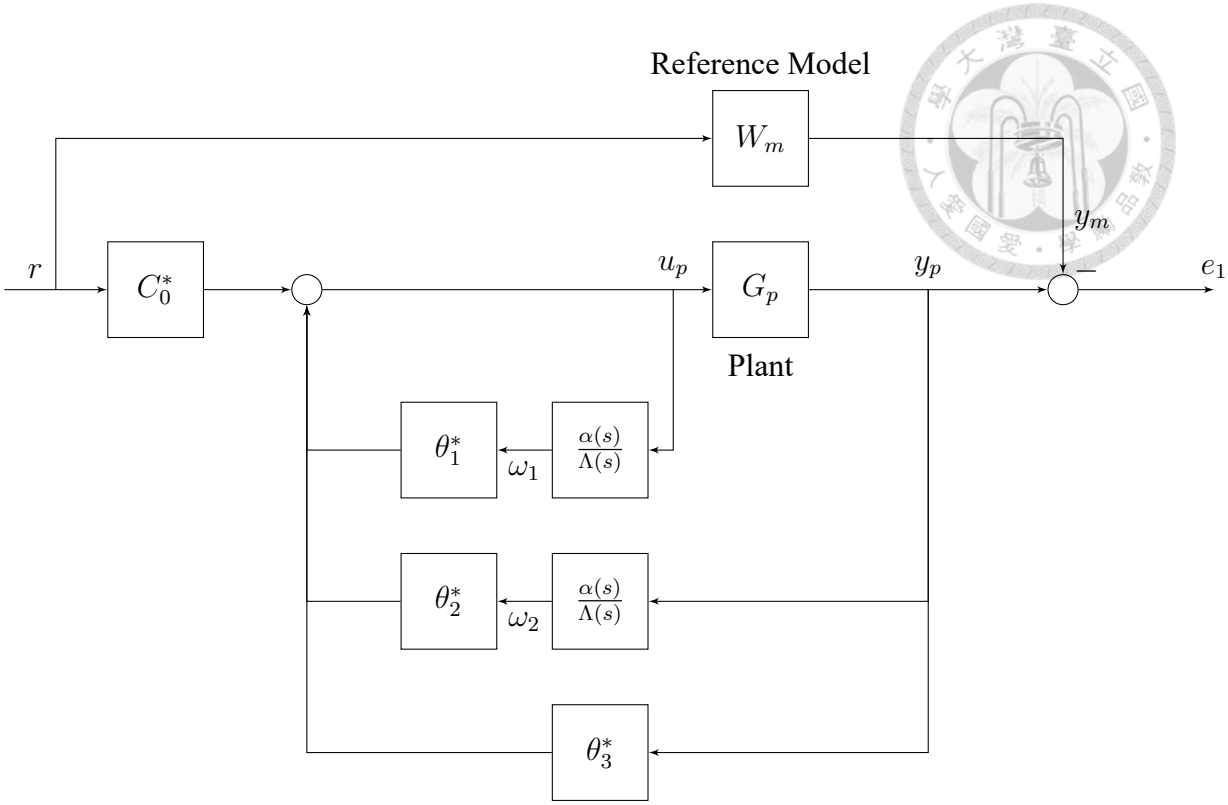

Figure 3.6: Schematic block diagram of *MRAC*

been utilized on a stationary circular cylinder in the previous research to attenuate the lift fluctuation [15].

3.4 Model Reference Adaptive Control

Model reference adaptive control (MRAC) is one class of adaptive control. *MRAC* applies the adaptive law to the parameter tuning based on the structure of *Model reference control (MRC)*. In *MRC*, a linear time-invariant system (LTI system) is chosen as the reference model for a desired output y_m under the reference input r. Figure 3.6 shows the relation between the reference model and the real plant. If the plant G_p is a known transfer function, the model reference control problem becomes a model-matching problem. On the other hand, if the plant G_p is unknown or we only have mere knowledge about the relative degree of the transfer function, the adaptive law has to be introduced to solve the

doi: 10.6342/NTU202301391

design problem. Since the Resolvent operator is initially computed based on the uncontrolled time average baseflow, the operator is expected to change concerning the additional controller. This concept is similar to the idea of iterative control performed by Leclercq *et al.*(2019)[16]. They updated the controller with respect to the new equilibrium state after appending the old controller. In *MRAC*, the concept is similar. The plant is supposed to be unknown, but a controller will be designed adaptively to minimize the tracking error $e_1 = y_p - y_m$ for the given reference input r. The Resolvent operator based on the linearization of the baseflow of the stationary cylinder is designated as the reference model. It is expected that the adaptive controller can synchronize the mean flow of the plunging case with the unplugging one. Consequently, the fluctuation of the lift coefficient could be diminished due to the change in the average base flow.

Before examining the effect of adaptive control, an effective adaptive law for estimating control parameters has to be established. The direct adaptive algorithm is adopted here, which directly updates the controller parameters $\theta_c = [c_0, \theta_1^T, \theta_2^T, \theta_3]^T$ without first estimating the unknown plant parameters. The corresponding control law is written as follows.

$$u_p = c_0(t)r + \theta_1^T(t)\frac{\alpha(s)}{\Lambda(s)}u_p + \theta_2^T(t)\frac{\alpha(s)}{\Lambda(s)}y_p + \theta_3(t)y_p \tag{3.18}$$

where u_p is the control input, y_p is the plant output, and the $\frac{\alpha(s)}{\Lambda(s)}$ represents the stable filter. The state-space realization of the equation (3.18) is

$$\begin{aligned} \dot{\omega_1} &= F\omega_1 + gu_p, \\ \dot{\omega_2} &= F\omega_2 + yu_p, \\ u_p &= \theta_c^T\omega,\ \omega = [r, \omega_1^T, \omega_2^T, y_p] \end{aligned} \tag{3.19}$$

doi: 10.6342/NTU202301391

, where (F, g) is the state-space realization of $\frac{\alpha(s)}{\Lambda(s)}$, which can be conducted by various canonical forms. Ioannou and Fidan [14] further defined the cost function J, which should be minimized to achieve the goal of tracking model reference signal.

$$J(\rho, \theta) = \frac{(e_1^* - e_1)^2}{2m_s^2} = \frac{(e_1^* - e_1)^2}{2(1 + \phi^T\phi + (W_m(s)u_p)^2)}, \tag{3.20}$$

where $\phi = -W_m(s)\omega$ and e_1^* is the desired error output with the desired feedback gain θ_c^*. By applying the gradient method, the normalized adaptive laws can be written as

$$\begin{aligned}
\dot{\theta}_c &= -\Gamma\nabla J_\theta = \Gamma\frac{e_1 - \rho(\theta_c^T\phi + W_m u_p)}{1 + \phi^T\phi + (W_m u_p)^2}\phi\text{sgn}(\frac{k_p}{k_m}) \\
\dot{\rho} &= -\gamma\nabla J_\rho = \gamma\frac{e_1 - \rho(\theta_c^T\phi + W_m u_p)}{1 + \phi^T\phi + (W_m u_p)^2}(\theta_c^T\phi + W_m u_p) \\
\phi &= -W_m(s)\omega
\end{aligned} \tag{3.21}$$

, where $e_1 = y_p - y_m$ is the tracking error of the plant output. More specifically, the hyperparameters, Γ and γ, should be positive-definite matrices in the adaptive control. It will result in a high-dimensional optimization problem. To simplify the optimization process, diagonal matrices composed of Γ and γ as the diagonal terms are adopted. That is to say, Γ and γ, which are now two scalar constants, must be chosen primarily as the learning rate of the adaptive laws. The two parameters, therefore, could be used to obtain the optimal control performance. In summary, the above adaptive laws provide a way to directly tune the control variables θ_c to adapt to the unknown plant in the flow system to minimize the difference between the plant output and reference output.

doi: 10.6342/NTU202301391

Chapter 4 Result and Discussion

In this chapter, the control results conducted via the loop-shaping method and model-reference active control will be presented and compared with each other. This chapter aims to elucidate the detail of the controller synthesis and the control results in the nonlinear flow field. The content is organized as follows. In section 4.1, the result of the robust control is presented. In the section 4.2, the outcome of model reference adaptive control is shown. Lastly, the overall discussion regarding the two approaches is included in the section 4.3.

4.1 Loop-Shaping Method

In the loop shaping method, the objective is to achieve the desired shape of the open-loop transfer function PK in the frequency spectrum. Throughout the synthesis procedure, the closed-loop characteristic is expected to reject the input disturbance to achieve the ideal robust control performance. Specifically, the sensitivity function S will be investigated because the transfer function between the nonlinear forcing to the output is $T_{d\to y} = PS$. If the transfer function $T_{d\to y}$ consists of lower gain across the frequency spectrum, the flow field is more likely to be suppressed because of the weaker amplifying mechanism of the nonlinear forcing. In this thesis, the robust controllers are designed by

doi: 10.6342/NTU202301391

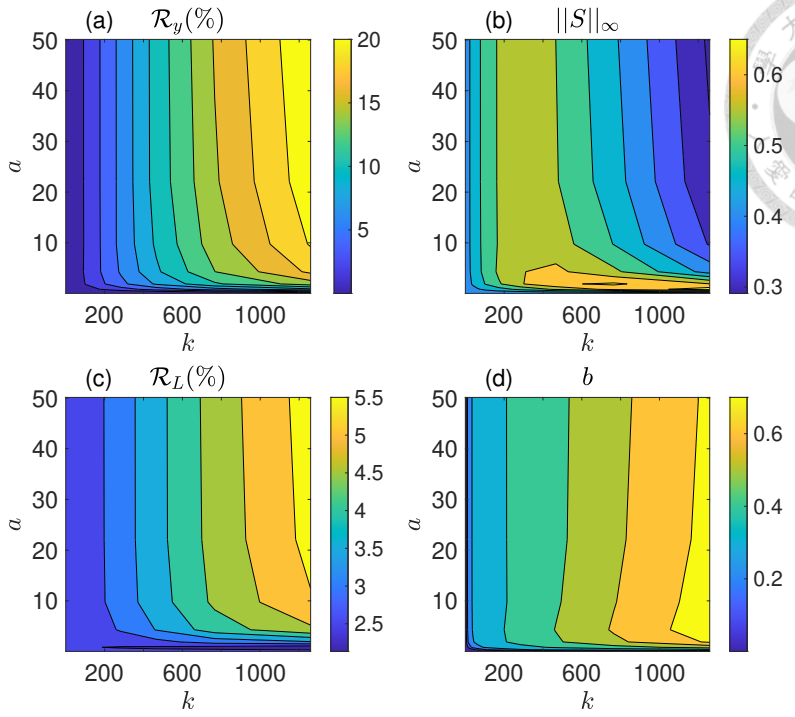

Figure 4.1: The relative fluctuation reduction and the stability margin predicted by the loop-shaping method. (a) The relative transverse velocity fluctuation reduction. (b) The infinite norm of the sensitivity function (c)The relative lift fluctuation reduction. (d) the normalized coprime stability margin b

choosing the parameters, k and a, in the weight function W. Since there are only two parameters, the optimization can be displayed visually with a two-dimensional contour plot shown in figure 4.1.

First of all, the graph of the stability margin shows that the gain of the weight function k plays a significant role in the robustness of the controlled system compared with the peak frequency a. The margin increases with the increment of the gain. Moreover, the trend is similar concerning the $\mathcal{H}$-infinity norm of the sensitivity function S. The norm decreases with the increasing gain. The fact demonstrates that the closed-loop system is more capable of rejecting the disturbance if the weight function is set up with a large enough gain k. However, it is worth noticing that the controller would become unstable with the increasing gain, even with a lower $\mathcal{H}$-infinity norm and larger stability margin. Hence, to implement the controller in the nonlinear flow, the design of the weight function should

doi: 10.6342/NTU202301391

be considered to have the upper bound for the gain. Nonetheless, the above analysis is basically linear based on the loop-shaping method. Since the control objective is the fluctuation reduction for the cylinder in a nonlinear flow field, the result should eventually be examined under the nonlinear simulation.

The control results in a nonlinear simulation are also presented in figure 4.1. The control effect on the fluctuation reduction is quantified by the new variable $\mathcal{R}_x$ for a time-series data x defined as follows.

$$\mathcal{R}_x = \frac{S_x^{\text{base}} - S_x^{\text{control}}}{S_x^{\text{base}}}, S_x = \sqrt{\frac{1}{N-1}\sum_{i=1}^{N}(x_i - \bar{x})^2}, \tag{4.1}$$

where the S_x is the standard deviation of the time-series data x with its average $\bar{x}$. In order to minimize the transient effect from the additional external forcing, time-series data x is collected after the control is appended for five plunging periods. According to the definition, $\mathcal{R}_x$ is positive when the fluctuation of the controlled flow has been suppressed by adding the controller. Two types of time-series data are shown here: the sensor output $\mathcal{R}_y$, which is the transverse velocity at the sensing location, and the lift coefficient $\mathcal{R}_L$. In summary, the two quantities should be maximized to accomplish the goal of fluctuation alleviation.

The fluctuation reduction of the transverse velocity, $\mathcal{R}_y$, is reduced with a maximum of 21.8% while the lift fluctuation reduction $\mathcal{R}_L$ is attenuated by 5.7%. The optimal case is shown in figure 4.2. After the actuator is turned on at the 10th period, the fluctuations of both velocity and lift have been reduced gradually. The lift coefficient fluctuation has been alleviated at most peaks. Moreover, the control input power is also needed to investigate to quantify the efficiency of the controller. For the optimal case displayed in figure 4.2, even with the optimal control performance, the power coefficient C_p of the two actua-

doi: 10.6342/NTU202301391

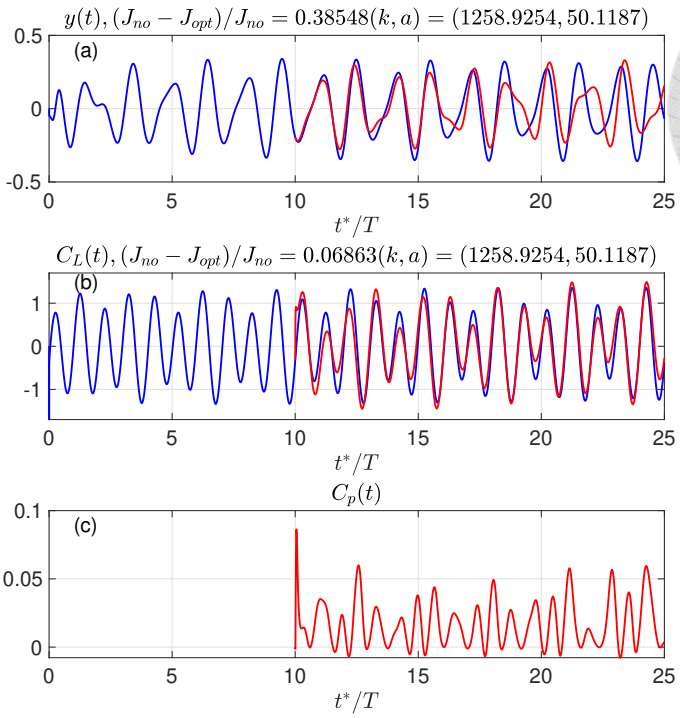

Figure 4.2: Lift and transverse velocity time-sequence data with the optimal loop-shaping-based controller. $\mathcal{R}_L = 5.7\%$, $\mathcal{R}_y = 21.8\%$ (a) The transverse velocity $y(t)$. (b) The lift coefficient $C_L(t)$ (c) The total power coefficient C_p of the two actuators with respect to the normalized time t^*/T, T is the plunging period. The red line represents the controlled case. The blue one denotes the base flow

tors is limited to 5% of the inflow power per unit area $\frac{1}{2}\rho U^3$. This low input power shows that the controller has efficiently utilized the intrinsic instability mechanism existing in the flow field to achieve the objective. This outcome agrees with the Resolvent analysis presented in section 3.1. The dominant forcing mode in Resolvent analysis implies that the external forcing on the angle $\theta_c = 110°$ is more likely to amplify throughout the linear operator.

Besides the optimal cases, the trends are also significant to demonstrate the efficacy of the control method for the periodic-oscillating boundary. With the increasing gain of the weight function, both fluctuation reduction quantities $\mathcal{R}_y$, and $\mathcal{R}_L$ decrease accordingly. This trend is similar to the H-infinity norm of the sensitivity function and the stability margin b predicted prior by the linear control theory. This discovery offers the potential of robust control theory on flow control with harmonic-oscillating boundaries. Instead

doi: 10.6342/NTU202301391

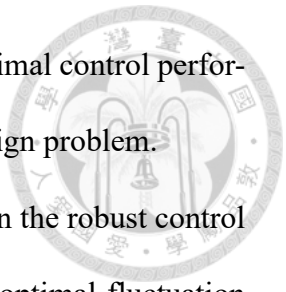

of optimizing throughout the heavy-cost nonlinear simulation, the optimal control performance can be predicted by the fast algorithm of the linear control design problem.

To summarize, I have proposed an effective control approach based on the robust control theory to stabilize the flow field with an oscillating boundary. The optimal fluctuation reduction can be achieved 21.8% for the transverse velocity in the wake and 5.7% for the lift exerted on the cylinder. Moreover, the result conducted in the nonlinear simulation is consistent with the linear analysis predicted prior with the $\mathcal{H}$-infinity norm of sensitivity function and the stability margin for the closed-loop system. This outcome provides support for the further control design for the flow field with harmonic-oscillating boundaries. Although the flow field is highly nonlinear and high-dimensional, we could still rely on the reduced-order linear model to design an effective controller to attenuate the fluctuation and predict its efficacy. However, the linear plant is only valid to model the dynamics not far from the linearization point. That is to say that, due to the limit of the linear plant, the goal of fluctuation alleviation is constrained to around 5%. To further suppress the oscillation, an adaptive control method is introduced to solve the issues mentioned above in section 4.2.

4.2 Model Reference Adaptive Control

In the controller synthesis via *MRAC* , the reference model has to be determined prior. In this section, the resolvent operator of the stationary case is chosen as the linear reference model for the following design problem. The reason behind this choice lies in the motivation of the fluctuation reduction. Since the resolvent operator obtained from the stationary cylinder flow is a Hurwitz matrix, it is expected the response of the linear plant is bounded. Moreover, in the formulation of the resolvent operator, the nonlinear forcing

doi: 10.6342/NTU202301391

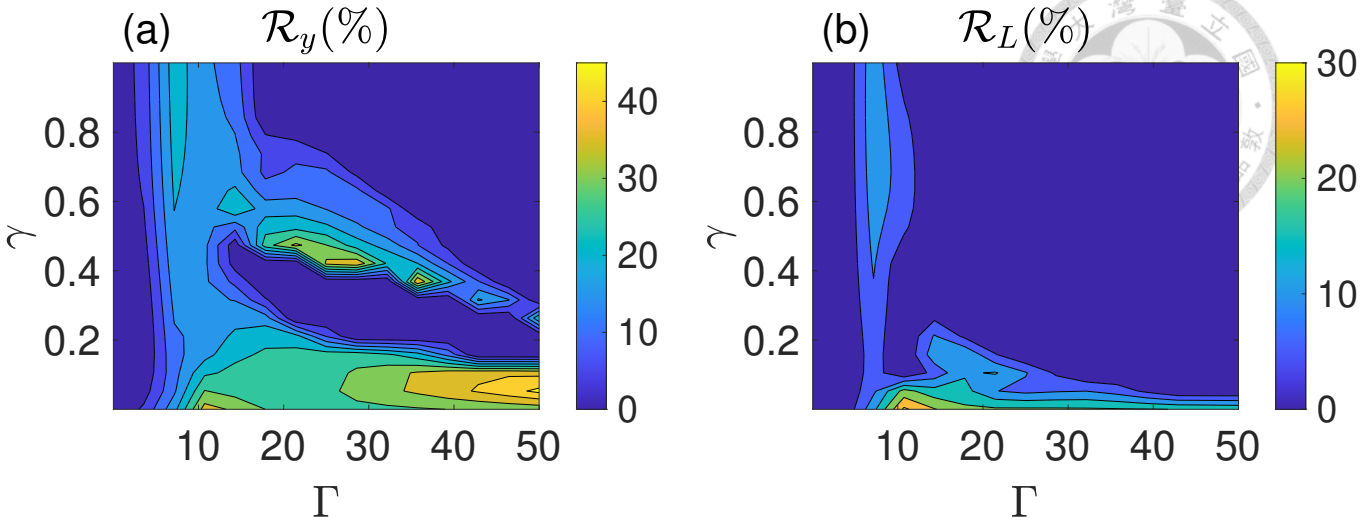

Figure 4.3: The relative fluctuation reduction $\mathcal{R}$ via the model reference adaptive control. (a) The fluctuation reduction of transverse velocity at sensing points. (b) The fluctuation reduction of lift on the circular cylinder

plays a role in sustaining the harmonic oscillation of the flow response in the plunging cylinder flow. The nonlinear forcing includes the periodic terms originating from the oscillating boundaries. Therefore, since the input of the reference model does not include the nonlinear forcing, the adaptive controller is expected to suppress the contribution of nonlinear forcing in the real system by minimizing the error between the plant output and the reference output. As a result, the fluctuation of lift and velocity will be reduced. Furthermore, in the feedback structure shown in figure 3.6, the filter $\frac{\alpha(s)}{\Lambda(s)}$ is also needed to be determined. The filter is set to be $\frac{1}{s+1}$ for the requirement of the adaptive control theory [14].

Secondly, the two hyperparameters, Γ and γ, should also be determined before the control implementation. Specifically, the parameter Γ represents the learning rate of the adaptive gains θ. As stated in the chapter 3, the parameter Γ generally is a positive-definite matrix, which represents the weight of each adaptive gain and the interaction among them. However, to simplify the discussion, a single learning rate is assigned to all the adaptive gains. Therefore, the parameter Γ is reduced to a scalar, as well as the parameter γ. Hence, the

doi: 10.6342/NTU202301391

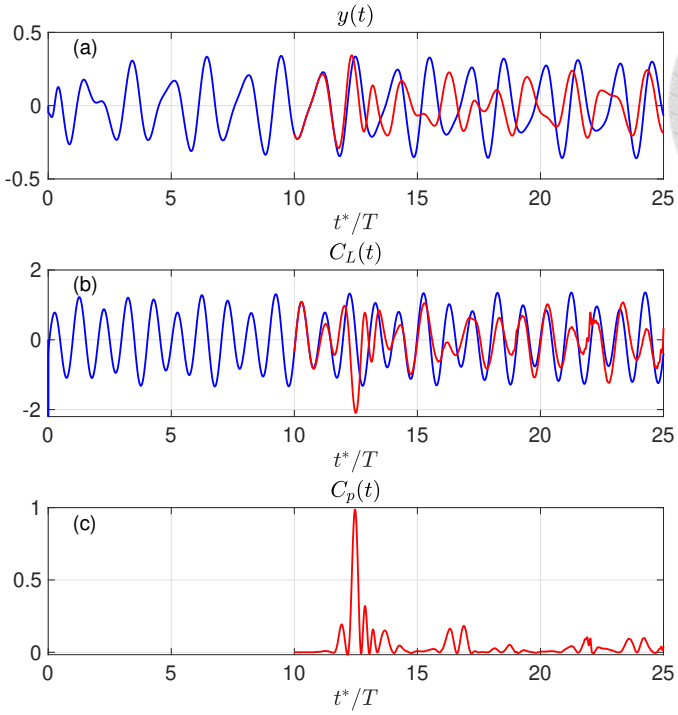

Figure 4.4: Lift and transverse velocity time-sequence data with the optimal adaptive controller. The control outcomes with the parameter pair $(\Gamma, \gamma) = (10.7, 10^{-4})$ are $\mathcal{R}_L$ = 30.9%, $\mathcal{R}_y$ = 37.2% (a) The transverse velocity. (b) The lift coefficient (c) The total power coefficient C_p of the two actuators with respect to the normalized time t^*/T , T is the plunging period. The red line represents the controlled case. The blue one denotes the base flow

optimization result can be shown in a two-dimensional graph with the two learning rates.

It is worth noticing that, in order to compare the two control methods, the definition of the relative fluctuation reduction $\mathcal{R}_i$ is set to be the same as the one in the section of the loop-shaping method, as well as the control horizon and the data collection interval. By conducting a plethora of control experiments with various parameter settings, a contour plot of control results with respect to the two parameters can be constructed as figure 4.3. First, the optimal result is clearly shown with a maximum of relative lift fluctuation reduction $\mathcal{R}_L = 30.9\%$ with a parameter pair $(\Gamma, \gamma) = (10.7, 10^{-4})$. The velocity fluctuation is also alleviated with a relative improvement of 37.2%. Second, the contour plot shows that the parameter γ should be limited to 0.2 to achieve fluctuation reduction. The trend is similar in both the velocity and lift fluctuation. Nonetheless, the effect of parameter Γ is

doi: 10.6342/NTU202301391

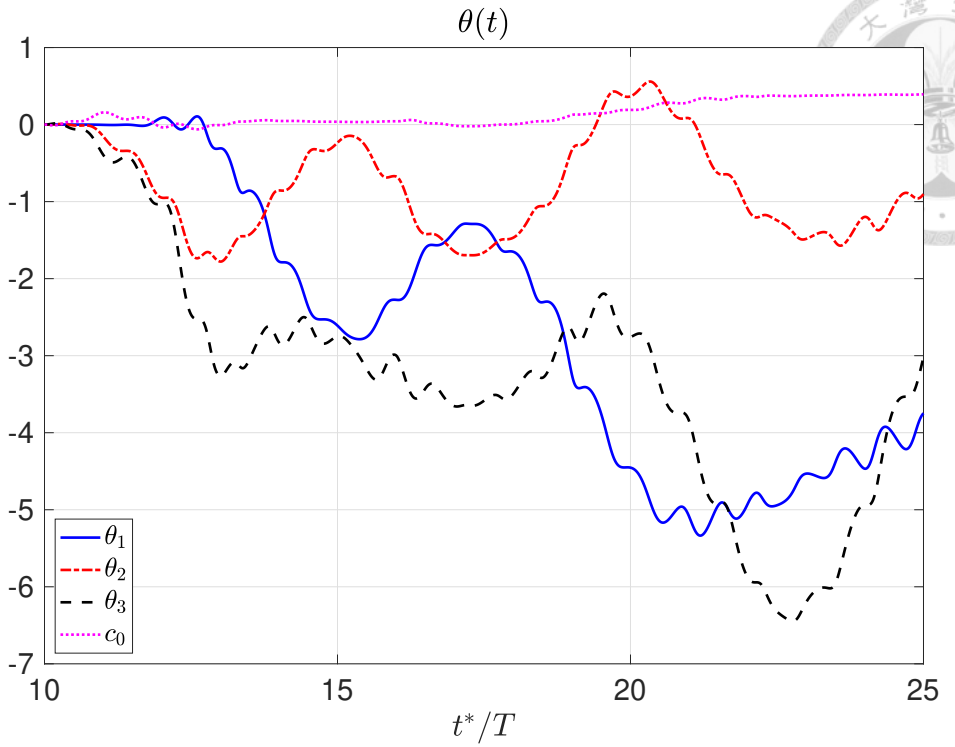

Figure 4.5: The time-series data of adaptive gains θ across the control horizon with the optimal setting $(\Gamma, \gamma) = (10.7, 10^{-4})$. $\theta_c = [\theta_1, \theta_2, \theta_3, c_0]$ in the equation 3.18

different in terms of the lift and the transverse velocity. The lift fluctuation attenuation is concentrated near $\Gamma = 10.7$, while the velocity alleviation reaches its maximum at $\Gamma = 50$.

By evaluating the optimal case shown in figure 4.4, several details of an adaptive controller can be demonstrated. First of all, the low learning rate of γ reflects on the transient data after the control implementation on $t^*/T = 10$. The controller has a minor influence on the flow field in the first three periods. However, around the third period, there is a burst in the power input, which means that a large amount of body force is required to be applied by the actuators. An adaptive controller's maximum power input requirement is larger than the one of a robust controller. This might be a drawback of the adaptive controller due to its constraint on the choice of actuators in the practical application. Nonetheless, the adaptive control approach delivers better performance on the lift fluctuation after the transient response. In figure 4.4, most peaks of the lift coefficient can be alleviated, which is hardly achieved by the robust control method.

doi: 10.6342/NTU202301391

Furthermore, the adaptive gains are investigated to study the convergence of the control method. The adaptive gains, $\theta_c = [\theta_1, \theta_2, \theta_3, c_0]$ represent respectively the feedback gain of the filtered control input, filtered plant output, unfiltered plant output, and the reference input. Theoretically, the gains will be able to converge to a static gain with which the closed-loop system can have the same output as the reference model. The theory guarantees that the statement is held for the linear plant. However, the real flow system consists of a great proportion of contribution from the nonlinearity. This disturbance will introduce uncertainty for the linear formulation of adaptive laws, leading to a non-asymptotically stable error signal. This conjecture can be supported by the gains in figure 4.5. For the gain of the reference input c_0, the adaptive laws guide the gain to converge to a single value. Nonetheless, the rest of the gains, $\theta_1, \theta_2, \theta_3$, do not converge. This outcome explains why the fluctuation could not be further attenuated as the reference output. The disturbance introduced by the nonlinearity and periodic forcing near the boundaries affects the convergence process of the adaptive gains.

4.3 Discussion

Two control methods are presented above, including robust control and adaptive control. For the loop-shaping method, since robust control theory only guarantees the maximum stability margin for the linearized nominal plant, the distance between the system states, and the equilibrium point is expected to limit the control performance. Once the states are shifted far enough from the original linearized state, the controller will lose its efficacy. Therefore, the maximum performance on attenuating lift fluctuation will be constrained. This concept is verified by the control result of the maximum 5.7 % improvement in the fluctuation alleviation. But how can we break this limit to reduce the fluctuation

doi: 10.6342/NTU202301391

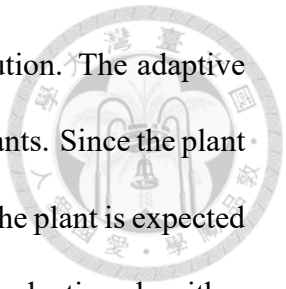

further? In this thesis, I believe that adaptive control will be the solution. The adaptive control theory design the controller to adapt to the different nominal plants. Since the plant is derived by linearizing the Navier-Stokes equation for the baseflow, the plant is expected to shift concerning the additional control input. That is to say that the adaptive algorithm supposes to, therefore, offer an approach to adjust the controller with respect to the new linear model. This conjecture is verified by the improvement in the fluctuation attenuation of 30.9 % by applying the *MRAC*. Although the adaptive control has better performance on the objective of fluctuation reduction, the higher demand for the actuator's maximum power input brings drawbacks to the method. On the other hand, the loop-shaping method provides a mild controller which has a lower maximum power input compared to the adaptive one.

doi: 10.6342/NTU202301391

Chapter 5 Conclusions and remarks

In this thesis, I have proposed two flow control approaches for a periodic-plunging cylinder wake flow. One is the loop-shaping method, and the other is the model reference adaptive control. My work mainly focuses on designing an effective controller that utilizes the two branches of control theory to attenuate the fluctuation induced by the oscillating motion of the boundary. The example presented in this thesis is a non-locking plunging cylinder. Due to the plunging motion in the transverse direction, the lift fluctuation is intensified more than the drag fluctuation. Consequently, the objective of the flow control is set to lift fluctuation reduction. First, the Resolvent operator based on the time-average flow is treated as the linear plant of the flow system. For the plunging cylinder wake flow, the Resolvent analysis provides support for the choice of actuator locations on the cylinder. The forcing mode suggests that the employment of external force near the separation point, which is 110° from the stagnation point to the actuating position on the cylinder, can be amplified most via the Resolvent operator and, therefore, achieve an energy-efficient controller.

With the result of the Resolvent analysis, I first develop a robust controller via the loop-shaping method. The approach optimizes the stability margin of the closed-loop system with a designated weighted open-loop transfer function. In the structure of the Resolvent-based linear system, the optimization leads to the ability to reject disturbance from the

doi: 10.6342/NTU202301391

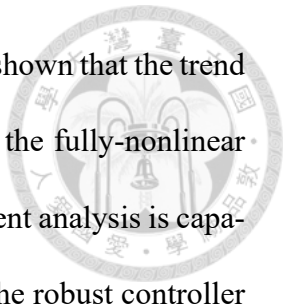

nonlinear forcing and periodic boundary forcing. In figure 4.1, I have shown that the trend of sensitivity function obtained from the linear analysis is similar in the fully-nonlinear simulation. This result shows that the linear plant obtained via Resolvent analysis is capable of designing a feedback controller. To conclude, the outcome of the robust controller synthesis not only results in the optimal lift fluctuation reduction of 5.7% but also shows that we can rely on the prediction based on the Resolvent operator via a simple linear analysis instead of a time-consuming nonlinear simulation.

To improve the control performance, the limit of a robust controller has to be examined. The robust controller is designed based on a known linear plant which is linearized upon the equilibrium state of the uncontrolled flow. However, the equilibrium state is expected to vary with the addition of actuators. Hence, the controller should be adaptively modified in different stages of control. To overcome this conundrum, the direct model reference adaptive control (*MRAC*) is introduced as the adaptive control scheme. With the direct *MRAC*, the control parameters can be directly adjusted for an unknown linear plant to track reference output. In this thesis, the unknown plant is the time-varying Resolvent operator in different stages of control. The optimal fluctuation reduction of this approach can achieve over 30% compared to the base flow. Nonetheless, one drawback must be mentioned. The maximum power requirement for an adaptive controller is larger than the one designed via robust control.

In summary, the two control methods proposed in this study have been verified to be effective in the fluctuation suppression for a flow field with harmonic oscillating boundaries. I first show that the Resolvent operator derived from a constant base flow could be used in the first stage of the control design. Furthermore, the limitation of the linear plant can be improved by introducing adaptive control. Nonetheless, the combination of the two ap-

doi: 10.6342/NTU202301391

proaches needs to be investigated to achieve both robustness and adaptiveness in a single controller.

doi: 10.6342/NTU202301391

doi: 10.6342/NTU202301391

References

[1] S. Bao, S. Chen, Z. Liu, J. Li, H. Wang, and C. Zheng. Simulation of the flow around an upstream transversely oscillating cylinder and a stationary cylinder in tandem. Physics of Fluids, 24(2):023603–023603–20, Feb. 2012.

[2] H. Choi, P. Moin, and J. Kim. Active turbulence control for drag reduction in wall-bounded flows. Journal of Fluid Mechanics, 262:75–110, 1994.

[3] J. Choi, T. Colonius, and D. R. Williams. Surging and plunging oscillations of an airfoil at low reynolds number. Journal of Fluid Mechanics, 763:237–253, 2015.

[4] T. Colonius and K. Taira. A fast immersed boundary method using a nullspace approach and multi-domain far-field boundary conditions. Computer Methods in Applied Mechanics and Engineering, 197(25):2131–2146, 2008. Immersed Boundary Method and Its Extensions.

[5] E. A. Deem, L. N. Cattafesta, M. S. Hemati, H. Zhang, C. Rowley, and R. Mittal. Adaptive separation control of a laminar boundary layer using online dynamic mode decomposition. Journal of Fluid Mechanics, 903:A21, 2020.

[6] S. Endrikat, D. Modesti, R. García-Mayoral, N. Hutchins, and D. Chung. Influence of riblet shapes on the occurrence of kelvin – helmholtz rollers. Journal of Fluid Mechanics, 913:A37, 2021.

doi: 10.6342/NTU202301391

[7] N. Fabbiane, B. Simon, F. Fischer, S. Grundmann, S. Bagheri, and D. S. Henningson. On the role of adaptivity for robust laminar flow control. Journal of Fluid Mechanics, 767:R1, 2015.

[8] T. L. B. Flinois and A. S. Morgans. Feedback control of unstable flows: a direct modelling approach using the eigensystem realisation algorithm. Journal of Fluid Mechanics, 793:41–78, 2016.

[9] D. Gatti and M. Quadrio. Reynolds-number dependence of turbulent skin-friction drag reduction induced by spanwise forcing. Journal of Fluid Mechanics, 802:553–582, 2016.

[10] K. Glover and D. C. McFarlane. Robust stabilization of normalized coprime factor plant descriptions with h/sub infinity /-bounded uncertainty. IEEE Transactions on Automatic Control, 34:821–830, 1989.

[11] G. Gómez-de Segura and R. García-Mayoral. Turbulent drag reduction by anisotropic permeable substrates –analysis and direct numerical simulations. Journal of Fluid Mechanics, 875:124–172, 2019.

[12] X. Hu and A. S. Morgans. Attenuation of the unsteady loading on a high-rise building using feedback control. Journal of Fluid Mechanics, 944:A10, 2022.

[13] J. I. Ibrahim, A. Guseva, and R. Garcia-Mayoral. Selective opposition-like control of large-scale structures in wall-bounded turbulence. Journal of Physics: Conference Series, 1522(1):012015, apr 2020.

[14] P. Ioannou and B. Fidan. Adaptive Control Tutorial. Society for Industrial and Applied Mathematics, Philadelphia, PA, 2006.

doi: 10.6342/NTU202301391

[15] B. Jin, S. J. Illingworth, and R. D. Sandberg. Feedback control of vortex shedding using a resolvent-based modelling approach. Journal of Fluid Mechanics, 897:A26, 2020.

[16] C. Leclercq, F. Demourant, C. Poussot-Vassal, and D. Sipp. Linear iterative method for closed-loop control of quasiperiodic flows. Journal of Fluid Mechanics, 868:26–65, 2019.

[17] T.-Y. Lin, H.-Y. Hsieh, and H.-C. Tsai. A target-fixed immersed-boundary formulation for rigid bodies interacting with fluid flow. Journal of Computational Physics, 429:110003, 2021.

[18] Q. Liu, Y. Sun, C.-A. Yeh, L. S. Ukeiley, L. N. Cattafesta, and K. Taira. Unsteady control of supersonic turbulent cavity flow based on resolvent analysis. Journal of Fluid Mechanics, 925:A5, 2021.

[19] M. Luhar, A. S. Sharma, and B. J. McKeon. Opposition control within the resolvent analysis framework. Journal of Fluid Mechanics, 749:597–626, 2014.

[20] B. J. McKEON and A. S. SHARMA. A critical-layer framework for turbulent pipe flow. Journal of Fluid Mechanics, 658:336–382, 2010.

[21] A. Padovan, S. E. Otto, and C. W. Rowley. Analysis of amplification mechanisms and cross-frequency interactions in nonlinear flows via the harmonic resolvent. Journal of Fluid Mechanics, 900:A14, 2020.

[22] E. Pickering, G. Rigas, O. T. Schmidt, D. Sipp, and T. Colonius. Optimal eddy viscosity for resolvent-based models of coherent structures in turbulent jets. Journal of Fluid Mechanics, 917:A29, 2021.

doi: 10.6342/NTU202301391

[23] M. QUADRIO, P. RICCO, and C. VIOTTI. Streamwise-travelling waves of spanwise wall velocity for turbulent drag reduction. Journal of Fluid Mechanics, 627:161–178, 2009.

[24] J. Rabault, M. Kuchta, A. Jensen, U. Réglade, and N. Cerardi. Artificial neural networks trained through deep reinforcement learning discover control strategies for active flow control. Journal of Fluid Mechanics, 865:281–302, 2019.

[25] D. Sipp. Open-loop control of cavity oscillations with harmonic forcings. Journal of Fluid Mechanics, 708:439–468, 2012.

[26] C. S. Skene, C.-A. Yeh, P. J. Schmid, and K. Taira. Sparsifying the resolvent forcing mode via gradient-based optimisation. Journal of Fluid Mechanics, 944:A52, 2022.

[27] D. Son and H. Choi. Iterative feedback tuning of the proportional-integral-differential control of flow over a circular cylinder. IEEE Transactions on Control Systems Technology, 27(4):1385–1396, 2019.

[28] C.-A. Yeh and K. Taira. Resolvent-analysis-based design of airfoil separation control. Journal of Fluid Mechanics, 867:572–610, 2019.

doi: 10.6342/NTU202301391